Science of the Total Environment 857 (2023) 159578

Contents lists available at ScienceDirect

Science of the Total Environment

journal homepage: www.elsevier.com/locate/scitotenv

Increasing role of phenolic oxidative branch in daytime oxidation process of aromatics in Chinese haze period

Fanglin Wang [a], Xiaodi Liu [a], Shaojun Lv [a], Si Zhang [a], Can Wu [a], Shijie Liu [a], Yali Lei [a], Yubao Chen [a], Rui Li [a], Gehui Wang [a,b,*]

[a] Key Lab of Geographic Information Science of the Ministry of Education, School of Geographic Sciences, East China Normal University, Shanghai 200241, China
[b] Institute of Eco-Chongming, Chenjia Zhen, Chongming, Shanghai 202150, China

HIGHLIGHTS

- Aromatics-associated VOC species were measured in 2019 winter on Chongming Island.
- Daytime secondary nitrophenols increased sharply under high NOx conditions.
- The RO_2 oxidative pathway dominated the aromatics oxidation on the non-hazy days.
- Phenolic oxidative branching ratios increased dramatically on the hazy days.

GRAPHICAL ABSTRACT

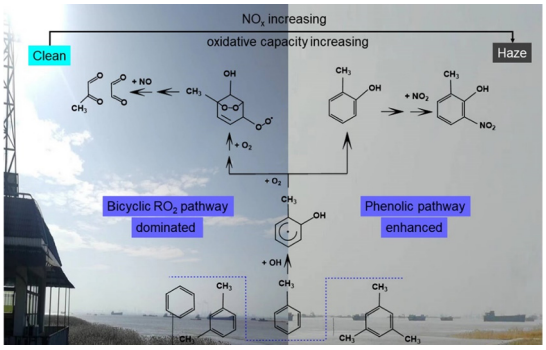

ARTICLE INFO

Editor: Pingqing Fu

Keywords:
VOCs
Aromatics oxidation pathway
Bicyclic RO_2 oxidation branch
Phenolic branch
High-NOx

ABSTRACT

To understand the photooxidation mechanisms of aromatic compounds in the NOx-rich atmosphere, gaseous aromatics and their oxidization products (i.e., methyl glyoxal (MGLY), and nitrated phenols (NPs) including nitrophenols (NPhs) and methylnitrophenols (MNPs)) were measured with a 1-h time resolution on Chongming Island, a downwind region of the Yangtze River Delta (YRD) metropolitans of China in winter 2019 by using a proton-transfer-reaction mass spectrometer (PTR-MS). During the entire observation period, concentrations of the measured VOCs were 9.6 ± 7.1 ppbv for aromatics, 118 ± 59 pptv for MGLY, 36 ± 10 pptv for NPhs, and 9.3 ± 2.8 pptv for MNPs, respectively. Secondary NPs (SNPs) accounted for only 19–24 % of the total nitrated phenols during the clean and transition periods but increased to 44 % of the total on the hazy days. Moreover, the daytime mixing ratios of SNPs increased along with an increasing NO_2 concentration during the clean and transition periods, but in the haze period the daytime SNPs first increased along with the increasing NO_2 levels and then increased much more sharply when NO_2 was >25 ppbv. Such highly proportional and sharply increased daytime SNPs in the haze period indicated an enhanced phenolic oxidation under the high NOx conditions. In addition, the lack of correlations between aromatics and MGLY, increased $MGLY_{aro}$ (MGLY produced by aromatics), and sharply increased ΔSNPs / Δ(benzene + toluene) further suggested that such an increasing role of the phenolic oxidative branch in the daytime oxidation process of aromatics during the YRD haze period was caused by the strong atmospheric oxidation capacity and the high level of NOx.

1. Introduction

Aromatics are the most significant anthropogenic volatile organic compounds (VOCs) in the troposphere, which are mainly emitted from fossil

* Corresponding author at: Key Lab of Geographic Information Science of the Ministry of Education, School of Geographic Sciences, East China Normal University, Shanghai 200241, China.
E-mail address: ghwang@geo.ecnu.edu.cn (G. Wang).

http://dx.doi.org/10.1016/j.scitotenv.2022.159578
Received 5 September 2022; Received in revised form 15 October 2022; Accepted 15 October 2022
Available online 18 October 2022

fuel combustion, gasoline evaporation, and solvent usage. The majority of aromatic organics have been identified as the precursors of secondary organic aerosols (SOA) and O_3 (Du et al., 2022; Gentner et al., 2017; Ng et al., 2007; Wang et al., 2016; Zhang et al., 2015). Previous studies reported that aromatics dominated the fall-winter SOA formation with a contribution of about 79 % in the Pearl River Delta region (Ding et al., 2012), and contributed about 40 % of intermediate vapors over China's megacities (Nie et al., 2022). Both aromatics and their oxidation products can significantly affect air quality and climate (Hoyle et al., 2009), as well as human health (Seinfeld and Pandis, 2006).

Photochemical oxidation mechanisms of aromatics have been intensively studied in laboratories, with most of them focusing on toluene (Atkinsin and Aschma, 1994; Atkinson, 2000; Garmash et al., 2020; Ji et al., 2017; Ng et al., 2007; Rodigast et al., 2017; Zaytsev et al., 2019). As seen in Fig. 1, the oxidation processes of aromatics are initiated by the OH radical addition first, and then, in atmospheric conditions, the produced OH-adducts can be further oxidized by means of the bicyclic RO_2 branch (I), phenolic branch (II), aldehyde branch (III), and epoxide branch (IV). Concentrations of O_2, OH and NOx, as well as the mass ratio of NOx/VOCs, are the key factors determining the further oxidative pathways of the OH-adducts (Birdsall and Elrod, 2011; Garmash et al., 2020; Ge et al., 2017; Tsiligiannis et al., 2019; Xu et al., 2020). The bicyclic RO_2 pathway is commonly thought to be dominant compared with the other three branches (Birdsall et al., 2010; Schwantes et al., 2017; Suh et al., 2003). However, due to the limitations such as short reaction times, high concentrations of reactants, lack of online measurement of reactants and products, and high wall loss during the laboratory studies on the aromatic oxidation process (Zhang et al., 2014), the above mechanisms are controversial, with 20 %–50 % carbon deficiency (Xu et al., 2020) and 30 %–50 % radical non-closure still unexplained (Lu et al., 2021). Recently, a few studies have reported an increased branching ratio of the phenolic oxidative pathway (Birdsall et al., 2010; Ji et al., 2017; Wu et al., 2014). Qi et al. (2020) recommended an overall cresol branching ratio of 0.42–0.53, while Ji et al. (2017) proposed that it is the phenolic pathway rather than the bicyclic RO_2 pathway that dominates the toluene oxidation. Schwantes et al. (2017) also pointed out that with increasing OH substitution on the aromatic ring, the phenolic oxidative branch occurs more rapidly than the bicyclic RO_2 formation. Moreover, numeric model simulations have also frequently underestimated O_3 and SOA concentrations and OH production by using these lab results (Birdsall and Elrod, 2011; Volkamer et al., 2006; Wyche et al., 2009), which can mainly be ascribed to the uncertain phenolic branching ratio derived from lab studies (Schwantes et al., 2017), as recent modelling simulations improved the modeled O_3 and SOA yields by increasing the branching ratio from 0.18 to 0.48 (Zhang et al., 2021), and the predicted O_3 levels by applying a phenolic branching ratio of 0.36 (Sarwar et al., 2011). However, none of these new oxidation mechanisms for the aromatic oxidation branching ratios have been confirmed under real atmospheric conditions, and the photooxidation mechanisms of aromatics in NOx-rich environments remain unclear, which thus presents a significant challenge in elucidating the environmental behavior of anthropogenic VOCs.

In this study, we measured gaseous products formed by the bicyclic RO_2 oxidative pathway and the phenolic oxidative pathway on Chongming Island in the Yangtze River Delta (YRD) region of China in winter 2019

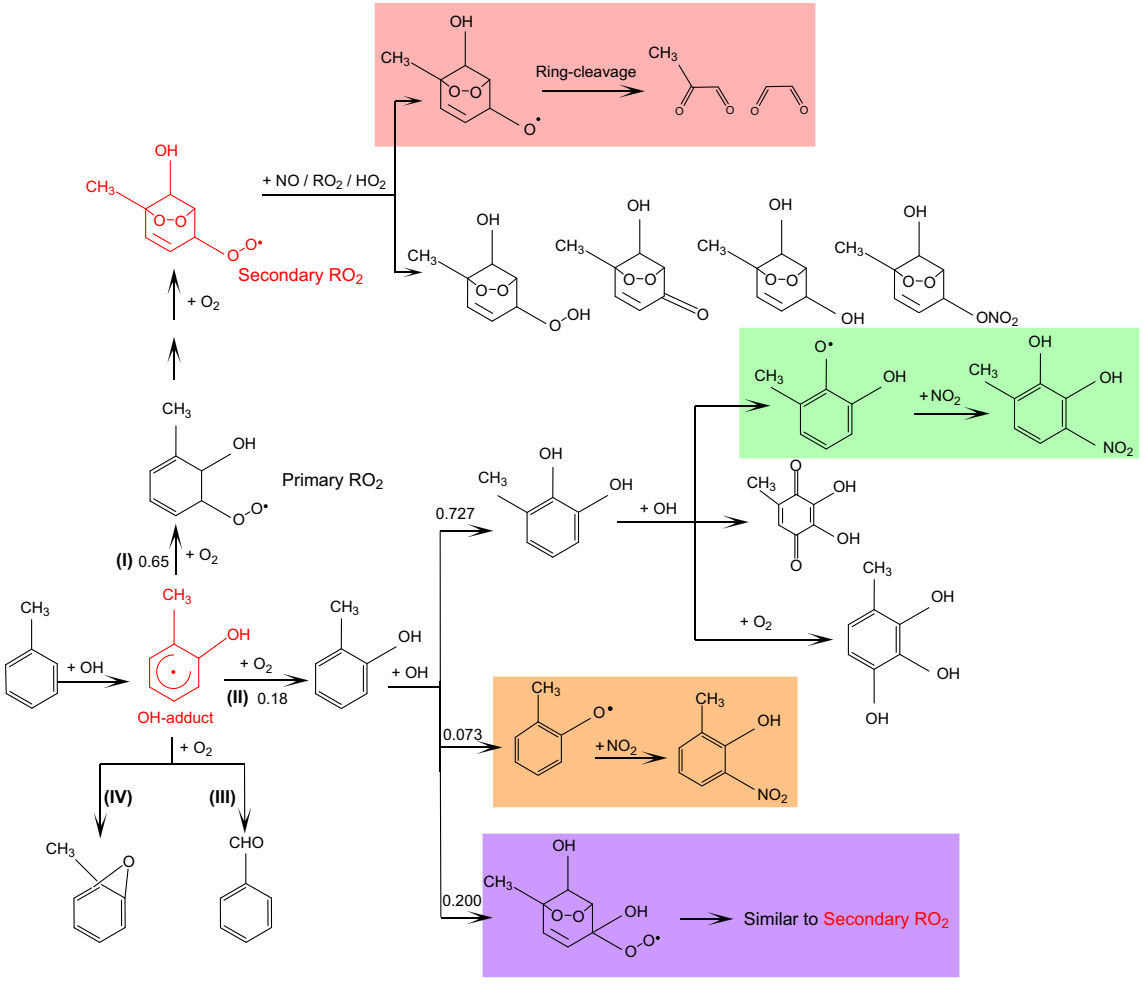

Fig. 1. Simplified representation of four oxidative pathways of OH-initiated aromatics in master chemical mechanism (MCM, http://mcm.york.ac.uk/). (I) bicyclic RO_2 pathway, (II) phenolic pathway, (III) aldehyde pathway, and (IV) epoxide pathway. For clarity, only toluene intermediates are shown.

with a 1-h time resolution. We first recognized the pollution characteristics of aromatics and their oxidation products in the haze period, and then investigated their oxidation mechanisms. Our work for the first time revealed an enhancing role of the phenolic branch in the daytime photooxidation process of aromatics in the NOx-polluted atmosphere.

2. Experiments

2.1. Sampling site

The sampling site is located in the ECNU Wetland Station (31°73′N, 121°24′E), which is located in the west part of Chongming Island, a downwind region of the Yangtze River Delta (YRD) megacities (Fig. S1), where there are no sources of pollutant emission around the sampling site. All the instrument inlets were mounted on the rooftop of the observation station with a height of six meters above the ground.

2.2. Experiment methods

Online measurements of VOCs, $PM_{2.5}$, HONO, NOx, CO, O_3, and SO_2 were simultaneously conducted from December 1st, 2019 to December 25th, 2019 (Du et al., 2022; Lv et al., 2022). Filter samples of $PM_{2.5}$ were also collected on a day/night basis (8:00 to 18:30 LT, local time, and 19:00 to7:30 in the next day, LT) by using a high-volume $PM_{2.5}$ sampler (TISCH, USA) with an airflow rate of 1.13 $m^3 \cdot min^{-1}$and measured for OC, EC and nitro-aromatic compounds (NACs) (Ding et al., 2021). In the current work, NACs of $PM_{2.5}$ (i.e., 4-nitrophenol, 3-methyl-4-nitrophenol, 4-nitrocatechol, and 4-methyl-5-nitrocatechol) were analyzed by gas chromatography–mass spectrometry (GC/MS, Angelon 5895GCMSD, USA). Concentrations of NOx, CO, SO_2 and O_3 were obtained from the local Bureau of Meteorology of Chongming Island. Meteorological parameters were measured by an automatic weather station (MILOS520, Vaisala Inc., Finland). The 1-h concentration of $PM_{2.5}$ was measured by using the *E*-BAM $PM_{2.5}$ monitor. VOCs including acetonitrile, isoprene, aromatics (benzene, toluene, C8 aromatics, and C9 aromatics), phenols, cresols, nitrophenols (NPhs), methylnitrophenols (MNPs), acetone, and methylglyoxal (MGLY) were measured by using a proton transfer reaction time-of-flight mass spectrometer (PTR-TOF-MS, Ionicon Analytik, Innsbruck, Austria) with H_3O^+ as the ion source, which was operated under the controlled conditions of pressure (2.2 mbar), temperature (70 °C) and voltage (600 V) resulting in a field density ratio (E/N) of z135 Td. During the campaign, the PTR-TOF-MS instrument was calibrated weekly using standard gases (Ionicon Analytik, Innsbruck, Austria), with the MGLY calibration factor calculated by using the methylethyl ketone (MEK) calibration factor because they have a constant ratio (Michoud et al., 2018). The calibration factors of phenol and cresols were estimated from the calibration results of toluene and C8 aromatics (Cappellin et al., 2012; Yuan et al., 2016), resulting in an uncertainty of 34 % for phenol and 22 % for cresols, respectively. The detection limits of the measured VOCs were calculated using a signal-to-noise ratio of three (Yuan et al., 2017), and the calibration results are shown in Table S1.

2.3. Data processing

In this study, the production rate of NO_3 radical ($P_{(NO3)}$) was calculated on the basis of the measured NO_2 and O_3 concentrations by using the Eq. (R_1), as the reaction of NO_2 with O_3 is the sole source of NO_3 radical (Asaf et al., 2009; Wayne et al., 1991):

$$P_{(NO3)} = k[NO_2][O_3], \quad \text{(R1)}$$

where k is 3.2×10^{-17} molec.$^{-1}$ cm^3 s^{-1}, and $[NO_2]$ and $[O_3]$ are the concentrations of NO_2 and O_3, respectively (Sander et al., 2011).

The secondarily formed NPs on Chongming Island during the campaign was estimated based on the following method (Li et al., 2019; Salvador et al., 2021; Zhang et al., 2019):

$$[SNP_s] = [NP_s] - \left(\frac{[NP_s]}{[tracer]}\right)_p \times [tracer], \quad \text{(R2)}$$

where $[SNP_s]$ and $[NP_s]$ are the concentrations of secondarily formed NPs and total NPs, respectively. $\left(\frac{[NP_s]}{[tracer]}\right)_p$ is the primary emission ratio of NPs to the primary tracer, and $[tracer]$ is the concentration of the selected primary emission tracer. In this study, $\left(\frac{[NP_s]}{[tracer]}\right)_p$ was estimated through fitting the 15 % lowest $\frac{[NP_s]}{[tracer]}$ ratios by using acetonitrile as the tracer of biomass burning, while CO, SO_2, and NO were used as tracers for estimating other primary emissions (Chen et al., 2022).

3. Results and discussions

3.1. Overview for the whole campaign

Temporal variations of aromatics and their oxidation products on Chongming Island during the campaign are shown in Figs. 2 and S2, and their concentrations are statistically summarized in Table S2. The average concentration of $PM_{2.5}$ during the whole observation period was 43 ± 28 μg m^{-3} (Table S2), higher than the national first-class standard of 35 μg m^{-3} in China, indicating that particle pollution is still serious in the country. In this study, we categorized the observation time with a daily $PM_{2.5}$ > 75 μg m^{-3} as haze event, the observation time with a daily $PM_{2.5} \leq$ 35 μg m^{-3} as clean period, and the remaining observation periods with a daily $PM_{2.5}$ between 35 μg m^{-3} and 75 μg m^{-3} as transition period. As marked in Fig. 2, during the campaign there were one haze period (12/8–12, gray color), two transition periods (12/2–6, and 12/13–15, orange color), and the remaining four clean periods (12/1–2, 12/6–8, 12/12–13, and 12/15–25, cyan color). It can be seen that concentrations of O_x ($O_x = O_3 + NO_2$) and HONO, as well as the values of $P_{(NO3)}$, increased along with increasing $PM_{2.5}$ levels and reached their maxima on the haze days (Fig. 2a, Fig. S2a), indicating that the atmospheric oxidation capacity was stronger in the haze period. The average concentration of aromatics was 9.6 ± 7.1 ppbv during the whole observation period and increased from 7.7 ± 2.7 ppbv in the clean period to 12 ± 4.0 ppbv and 13 ± 7.8 ppbv in the transition and haze periods, respectively (Fig. 2b, Table S2). Similarly, NOx increased obviously from the clean to the transition and haze periods, with a concentration ratio of NOx to aromatics of 1.1, 2.3 and 3.1 in the three phases, respectively, suggesting an NOx-rich condition on the haze days.

As displayed in Table S2, the average mixing ratio of MGLY was 118 ± 59 pptv during the whole observation period and increased from 100 ± 24 pptv in the clean period to 166 ± 100 pptv in the haze period. The temporal variation of MGLY was consistent with that of NOx and aromatics (Fig. 2c), indicating that both NOx and aromatics affect the MGLY levels. The mixing ratios of NPhs and MNPs were 35 ± 10 pptv and 9.3 ± 2.8 pptv during the whole campaign, respectively (Table S2). Compared to other regions, their concentrations were comparable to those in biomass burning influenced areas in Eastern China (the sum of NPhs and MNPs was 46.4 pptv) (Wang et al., 2020) but slightly lower than that in Beijing (NPhs and MNPs were 57 pptv and 17 ppbv, respectively) (Cheng et al., 2021). As shown in Fig. 1d, both NPhs and MNPs showed a similar temporal variation and were robustly correlated (R = 0.71 and 0.86, respectively, Fig. S3) with acetonitrile, indicating that they were significantly affected by biomass burning emissions in the YRD region (Mohr et al., 2013). By excluding the primary emission from biomass burning, we found that the secondarily formed NPhs (SNPhs) and MNPs (SMNPs) accounted for 18–25 % of the total during the clean and transition periods and sharply increased to 42 % and 46 % of the total NPhs and MNPs on the hazy days, respectively (see the concentric arc charts in Fig. 2d), indicating an increased formation

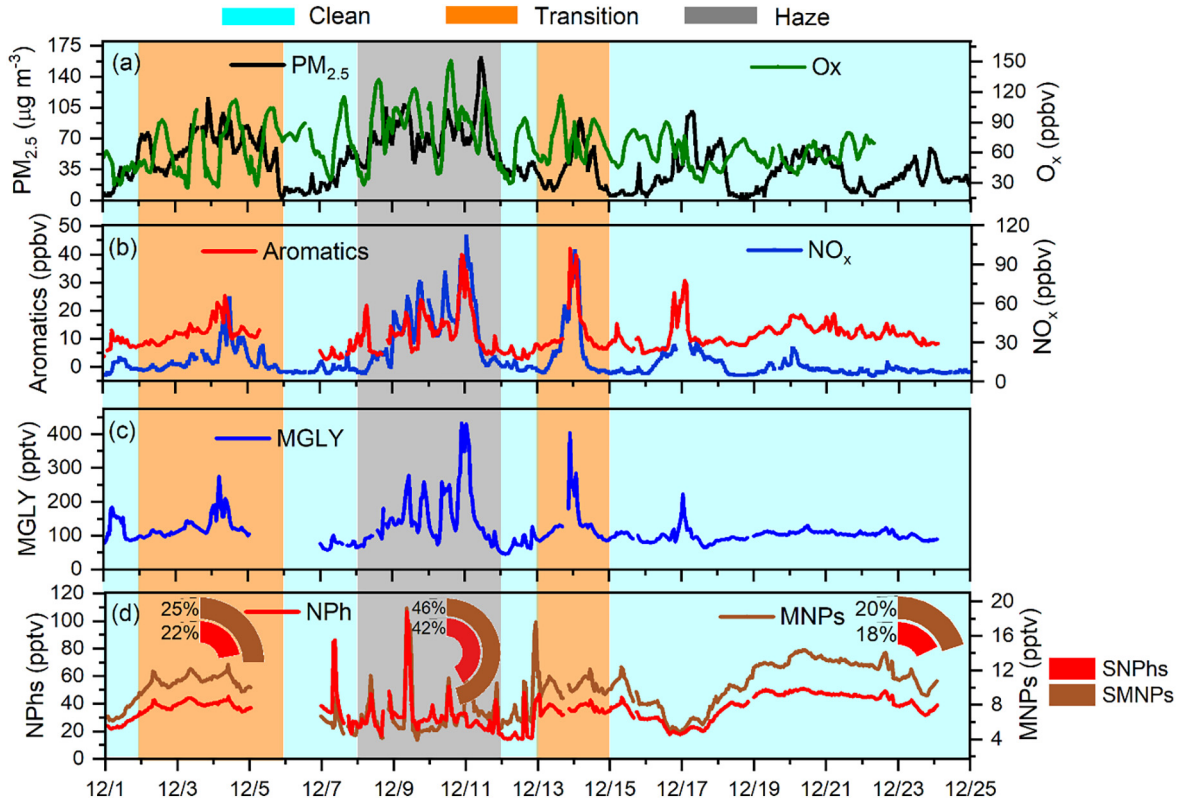

Fig. 2. Temporal variations in concentrations and compositions of volatile organic compounds during the whole observation period on Chongming Island, China. (a) $PM_{2.5}$ and O_x (O_x = O_3 + NO_2), (b) aromatics and NOx, (c) MGLY, (d) NPhs and MNPs in clean, transition, and haze periods. The blue, orange, and gray shadows represent the clean, transition, and haze periods, respectively.

of NPhs and MNPs in the haze period. Besides, the mixing ratios of daytime secondary NPs (SNPs, sum of SNPhs and SMNPs) increased along with NO_2 concentrations during the clean and transition periods, but in the haze period the daytime SNPs first increased along with the increasing NO_2 levels and then increased much more sharply when NO_2 was higher than 25 ppbv (Fig. 3), further suggesting an enhancement of daytime phenoxy or methylphenoxy radicals in the haze period under a high level of NOx conditions.

3.2. Diurnal variations of aromatics and their key oxidation products

Figs. 4 and S4 show the diurnal variations of aromatics and their key oxidation products during the clean, transition, and haze periods. As seen in Fig. 4a and b, the diurnal variations of aromatics and MGLY presented a similar pattern in the three periods, with an increase from 06:00 (local time, LT) to about 10:00 LT due to primary emissions, a decrease in the following hours due to photolysis and OH oxidation, and a sharp increase in the midnight due to the planet boundary layer shrinking (Ling et al., 2020). However, the diurnal variations of SNPhs and SMNPs are quite different in the three periods; both showed an insignificant diurnal change in the clean and transition periods but a remarkable diurnal variation in the haze period with a large peak in the morning and a second peak in the nighttime around 20:00 LT (Fig. 4c and d). The increases of SNPhs and SMNPs in the morning hours were due to the beginning of photochemical reactions, as indicated by the HONO concentration, which began to decrease at around 06:00 LT (Fig. S4e). The decrease during the daytime can be attributed to the fast photolysis or the reactions with OH radicals (Salvador et al., 2021; Yuan et al., 2016). These variations are similar to those reported from the Uintah Basin, USA (Yuan et al., 2016), Dezhou (Salvador et al., 2021) and Beijing (Song et al., 2021a), China. On Chongming Island in the haze period, the first increase in the morning can be attributed to the beginning of photochemical reactions like those in the clean and transition periods, whereas the increase starting in the late afternoon around 16:00 LT might be caused by the NO_3 radical

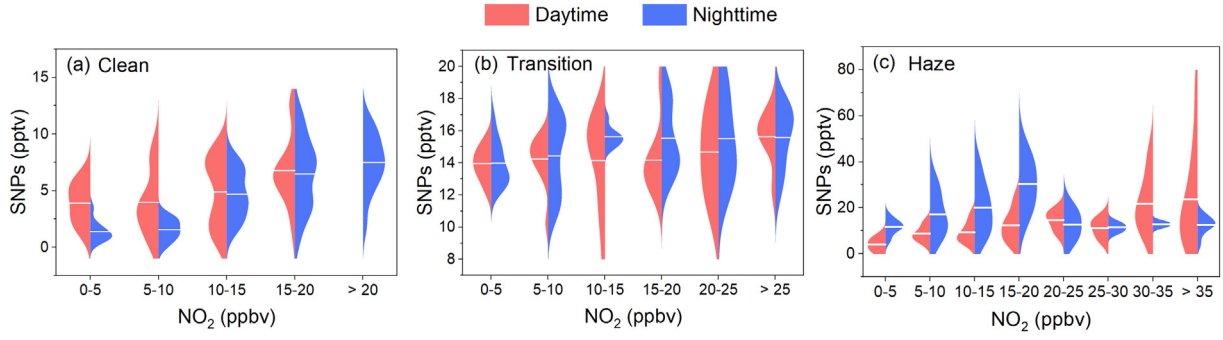

Fig. 3. Day-night mixing ratios of SNPs as a function of NO_2 concentration during the clean, transition and haze periods, respectively.

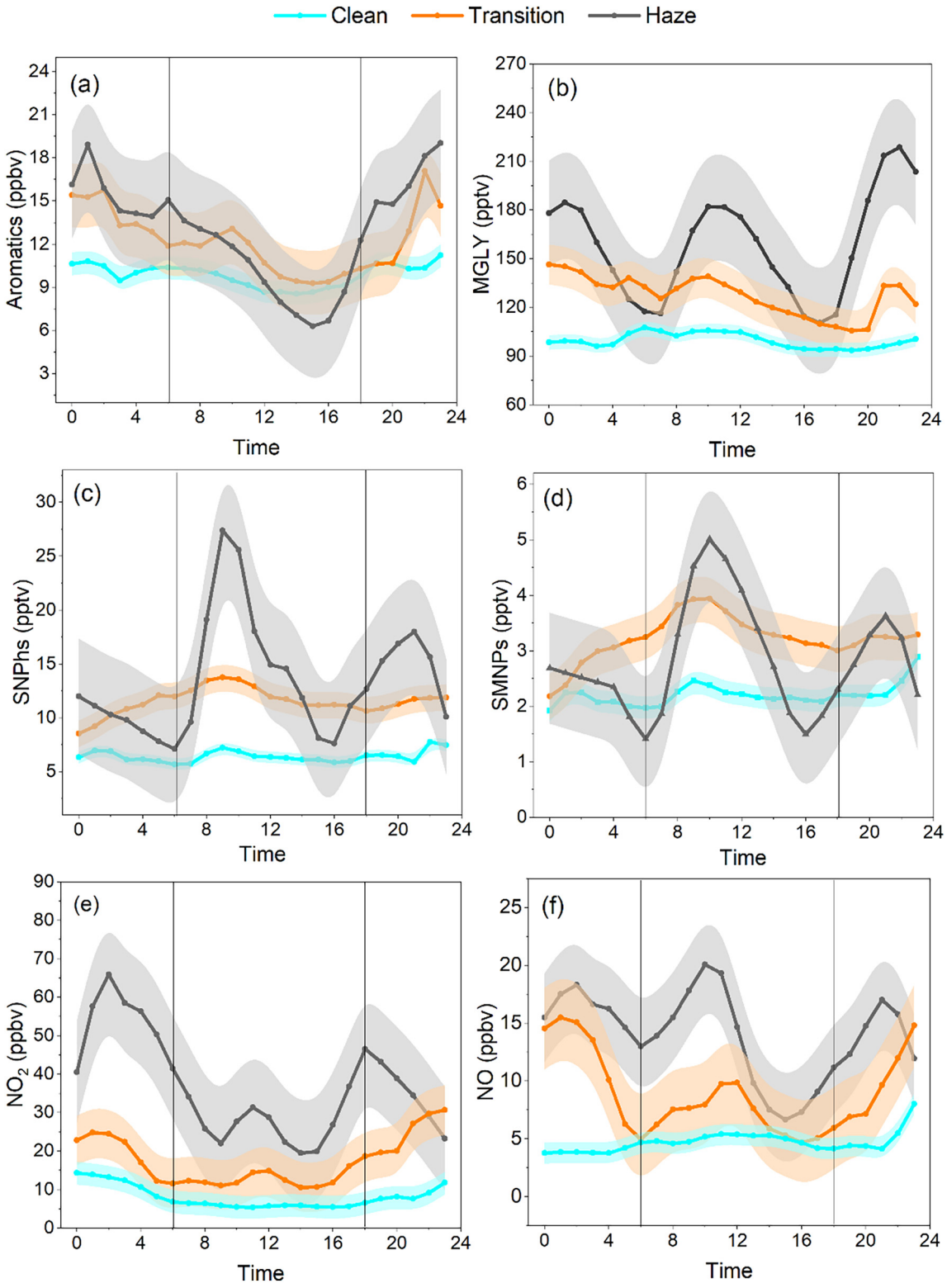

Fig. 4. Diurnal variations of (a) aromatics, (b) MGLY, (c) SNPhs, (d) SMNPs, (e) NO_2, and (f) NO during the clean, transition and haze periods, respectively.

oxidation due to the higher $P_{(NO3)}$ (Fig. S4f) and the lower NO concentration (Fig. 4f), since the reaction with NO is the largest sink of NO_3 radical (Asaf et al., 2009; Atkinson, 2000). Because the daytime NO_3 radical chemistry can only enhance daily SNPs mixing ratios in the late afternoon, the high production of SNPhs and SMNPs in the morning hours during the haze period might be caused by the different oxidation processes since the atmospheric oxidation capacity, NOx, and the mass ratio of NOx/aromatics were obviously different among the three periods.

3.3. Oxidative pathways of aromatics

As seen in Fig. 5, a robust linear correlation (R^2 = 0.60–0.92) between MGLY and the aromatics was observed during the clean and transition

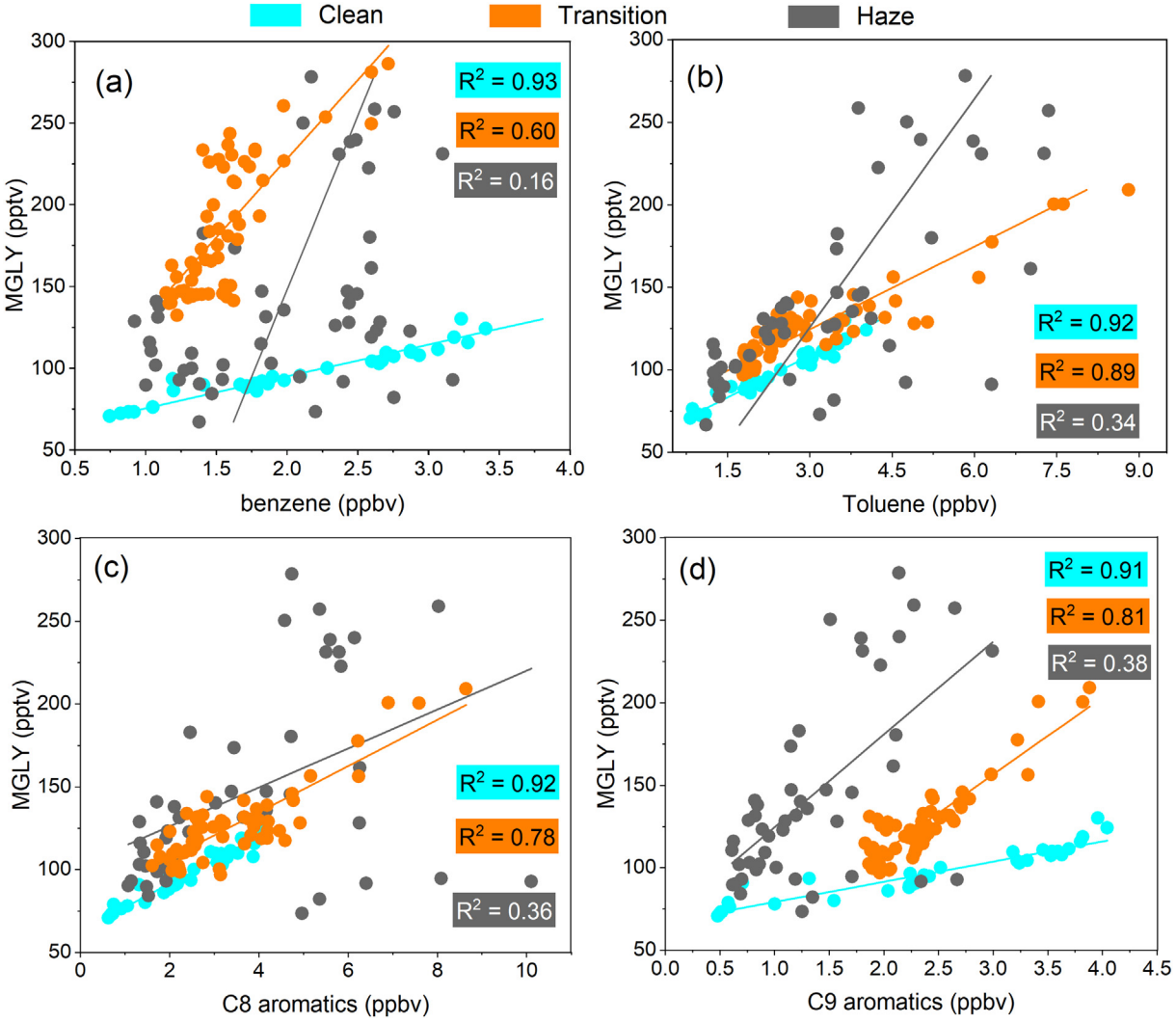

Fig. 5. Linear fit regression analysis for the daytime MGLY with (a) benzene, (b) toluene, (c) C8 aromatics, and (d) C9 aromatics during the clean, transition and haze periods, respectively.

periods, indicating a dominance of the bicyclic RO_2 branch in the two types of periods. However, no significant correlation was found during the haze period, suggesting that other oxidation pathways other than the bicyclic RO_2 pathway dominated the aromatic oxidation in the polluted period. According to the discussion in Section 3.1, the concentration of O_x in the haze event was 1.8 times higher than that in the clean period and 1.3 times higher than in the transition period, and the daytime NOx/aromatics ratio in the haze event was 2.1 times higher than that in the clean period and 3.3 times higher than in the transition period. Such a much stronger oxidative capacity and a higher NOx/aromatics ratio indicate that the oxidation pathway might be changed during the haze period since NOx controls the oxidation pathway by directly changing atmospheric oxidant levels and indirectly influencing RO_2 chemistry during the oxidation processes of aromatics (Schwantes et al., 2017; Tsiligiannis et al., 2019). In addition, the sharply increased phenols and cresols in the haze period (Fig. S2c, Table S2) indicated that the phenoxy and methylphenoxy radicals in the haze period also increased dramatically, which is in agreement with those observed by Song et al. (2021b), who also found that the measured phenoxy radical was about eight times higher in heavily polluted periods than on clean days. Based on the chamber experiment and quantum chemistry calculation, Ji et al. (2017) proposed that phenolic rather than bicyclic RO_2 oxidative pathway dominates the toluene oxidation under NOx-rich conditions. Schwantes et al. (2017) further reported that with increasing OH substitution on the aromatic ring, the phenolic oxidative branch occurs more rapidly than bicyclic RO_2 formation. Therefore, we assumed that the dominant oxidation pathway for aromatics may have changed from a bicyclic RO_2 oxidative pathway to a phenolic oxidative pathway on Chongming Island in the haze period, which led to the decrease in the association of MGLY with aromatics and the further dramatic increases in SNPs.

As seen in Fig. 6a, the daytime $MGLY_{aro}$ (MGLY produced by aromatics) decreased and ΔSNPs / Δ(benzene + toluene) increased slightly from the clean to the transition periods. The decreased $MGLY_{aro}$ could be attributed to the increasing NO_2 concentration in the transition period, as the yield of MGLY formed from the bicyclic RO_2 oxidative pathway decreases with increasing NO_2 levels (Noriko et al., 2010). The increase of ΔSNPs / Δ(benzene + toluene) could also be ascribed to the increasing NO_2 levels as the formation of SNPs was dependent on the NO_2 level (Yuan et al., 2016). However, both the daytime $MGLY_{aro}$ and ΔSNPs/Δ(benzene + toluene) ratio increased dramatically in the haze period (Fig. 6a). The SNPs originate from the reaction of the phenoxy or methylphenoxy radicals with NO_2 (marked in orange in Fig. 1), while the daytime phenoxy and methylphenoxy radicals are produced by the oxidation of phenol or cresol with OH (marked in orange in Fig. 1) and by the reaction of phenyl peroxy radicals and methylphenyl peroxy radicals with NO (marked in purple in Fig. 1) during the phenolic oxidative pathway. Studies have demonstrated that the reactions of phenyl peroxy radical and methylphenyl peroxy radicals with NO dominate the atmospheric daytime production of phenoxy and methylphenoxy radicals (phenoxy radical: beyond 71 % during

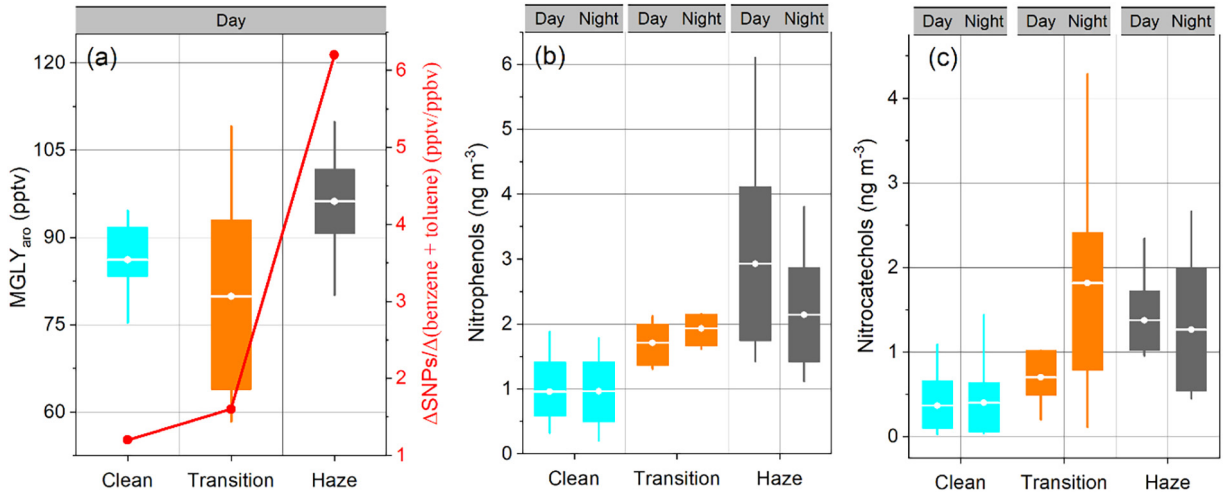

Fig. 6. A comparison on the different photooxidation chemistry in the clean, transition and polluted periods on Chongming Island, China. (a) Daytime $MGLY_{aro}$ and ΔSNPs / Δ(benzene + toluene), (b) nitrophenols in $PM_{2.5}$, and (c) nitrocatechols in $PM_{2.5}$.

daytime) (Cheng et al., 2021; Yuan et al., 2016). Thus, the dramatically increasing ΔSNPs / Δ(benzene + toluene) ratios indicate sharp increases of phenyl peroxy radicals and methylphenyl peroxy radicals through the enhanced phenolic oxidative pathway. Moreover, the phenyl peroxy radicals and methylphenyl peroxy radicals can further be broken into small α-carbonyl compounds, which are similar to those produced by the bicyclic RO_2 radicals (marked in red in Fig. 1), resulting in the $MGLY_{aro}$ increasing inversely in the haze period (Fig. 6a). In addition, the sharp increase of ΔSNPs / Δ(benzene + toluene) ratio and $MGLY_{aro}$ resulted by the enhanced phenolic oxidative pathway on the haze days in turn suggest that the insignificant correlation between aromatics and MGLY in the haze period was due to the differences in precursors and product generations; the MGLY was produced mainly by the aromatics-bicyclic RO_2 pathway (I, marked in pink color) in the clean and transition periods but by the phenolic-bicyclic RO_2 pathway (II, marked in purple color) in the haze period.

Fig. 6b and c compare the day-night variation of nitrophenols (sum of 4-nitrophenol and 3-methyl-4-nitrophenol) and nitrocatechols (sum of 4-nitrocatechol and 4-methyl-5-nitrocatechol) in the particle phase in the different periods on Chongming Island during the campaign. As shown in Fig. 1 (marked in green in Fig. 1), catechols, as the precursors of the nitrocatechols, are the major products of the phenolic oxidative pathway (MCM, http://mcm.york.ac.uk/). As seen from Fig. 6b and c, the daytime nitrophenols and nitrocatechols were lower than those in the nighttime during the clean and transition periods due to the loss of daytime photolysis and the higher yield and primary emission (Fig. S5) in the nighttime (Atkinson et al., 1992; Cheng et al., 2021). However, unlike those in the clean and transition periods, nitrophenols and nitrocatechols in the particle phase in the haze period were higher in the daytime than in the nighttime (Fig. 6b and c). Such an opposite diurnal variation pattern again demonstrated the enhanced role of the phenolic oxidative pathway in the daytime aromatic oxidation process on the hazy days in the YRD region.

4. Summary and conclusion

In this study, aromatics and their key oxidation products (i.e., MGLY and NPs) were continuously measured in winter on Chongming Island, YRD of China, to investigate the photooxidation process of aromatics under high-NOx conditions. Aromatics were 7.7 ± 2.7 ppbv, 12 ± 4.0 ppbv and 13 ± 7.8 ppbv with a mass ratio of NO_x to aromatics being 1.1, 2.3 and 3.1 in the clean, transition and haze periods, respectively, suggesting a NOx-rich condition on the haze days. The mixing ratio of MGLY, NPhs, and MNPs was 118 ± 59 pptv, 35 ± 10 pptv and 9.3 ± 2.8 pptv during the whole campaign, respectively. The secondarily formed NPhs and MNPs only accounted for 18–25 % the total NPhs and MNPs during the clean and transition periods but sharply increased to 42–46 % of the total on the hazy days, both of which presented a diurnal variation pattern different from those in the clean and transition periods with a large daytime peak on the hazy days, indicating the difference in the aromatic oxidation pathways in the polluted period. Differences in the correlation of aromatics with MGLY in the three periods and the sharp increase ratio of ΔSNPs / Δ(benzene + toluene) in the haze periods further suggest an enhanced role of phenolic oxidative pathway in daytime aromatic photooxidation process under the high-NOx conditions in the YRD region.

CRediT authorship contribution statement

Gehui Wang designed the whole research. Fanglin Wang conducted the experiment. Xiaodi Liu analyzed the filter samples. Fanglin Wang and Gehui Wang analyzed the data and wrote the paper. Other authors contributed to this work with helpful discussions.

Data availability

Data will be made available on request.

Declaration of competing interest

The authors declare that they have no known competing financial interests or personal relationships that could have appeared to influence the work reported in this paper.

Acknowledgements

This work was funded by Shanghai Science and Technology Innovation Action Plan (20dz1204011), the National Natural Science Foundation of China (No. 42130704), the programs from the Institute of Eco-Chongming and ECNU Happiness Flower Projects.

Appendix A. Supplementary data

Supplementary data to this article can be found online at https://doi.org/10.1016/j.scitotenv.2022.159578.

References

Asaf, D., Pedersen, D., Matveev, V., et al., 2009. Long-term measurements of NO3 radical at a semiarid urban site: 1. Extreme concentration events and their oxidation capacity. Environ. Sci. Technol 43, 9117–9123.

Atkinsin, R., Aschma, S., 1994. Products of the gas-phase reactions of aromatic hydrocarbons: effect of NO2 concentration. Int. J. Chem. Kinet. 26, 929–944.
Atkinson, R., 2000. Atmospheric chemistry of VOCs and NOx. Atmos. Environ. 34, 2063–2101.
Atkinson, R., Aschmann, S., Arey, J., 1992. Reactions of OH and NO3 radicals with phenol, cresols, and 2-nitrophenol at 296 ± 2 K. Environ. Sci. Technoi. 26, 1397–1403.
Birdsall, A., Elrod, M., 2011. Comprehensive NO-dependent study of the products of the oxidation of atmospherically relevant aromatic compounds. J. Phys. Chem. A 115, 5397–5407.
Birdsall, A., Andreoni, J., Elrod, M., 2010. Investigation of the role of bicyclic peroxy radicals in the oxidation mechanism of toluene. J. Phys. Chem. A 114, 10655–10663.
Cappellin, L., Karl, T., Probst, M., et al., 2012. On quantitative determination of volatile organic compound concentrations using proton transfer reaction time-of-flight mass spectrometry. Environ. Sci. Technol. 46, 2283–2290.
Chen, Y., Zheng, P., Wang, Z., et al., 2022. Secondary formation and impacts of gaseous nitrophenolic compounds in the continental outflow observed at a background site in South China. Environ. Sci. Technol. 56, 6933–6943.
Cheng, X., Chen, Q., Li, Y., et al., 2021. Secondary production of gaseous nitrated phenols in polluted urban environments. Environ. Sci. Technol. 55, 4410–4419.
Ding, X., Wang, X., Gao, B., et al., 2012. Tracer-based estimation of secondary organic carbon in the Pearl River Delta, South China. Journal of Geophysical Research: Atmospheres 117.
Ding, Z., Du, W., Wu, C., et al., 2021. Summertime atmospheric dicarboxylic acids and related SOA in the background region of Yangtze River Delta, China: implications for heterogeneous reaction of oxalic acid with sea salts. Sci. Total Environ. 757, 143741.
Du, W., Ding, Z., Lei, Y., et al., 2022. Atmospheric fine particulate dicarboxylic acids and related SOA in winter at the background site of Yangtze River Delta: implication for the long-distance transport of solid fuels burning. Atmos. Environ. 289, 119320.
Garmash, O., Rissanen, M., Pullinen, I., et al., 2020. Multi-generation OH oxidation as a source for highly oxygenated organic molecules from aromatics. Atmos. Chem. Phys. 20, 515–537.
Ge, S., Xu, Y., Jia, L., 2017. Secondary organic aerosol formation from propylene irradiations in a chamber study. Atmos. Environ. 157, 146–155.
Gentner, D., Jathar, S., Gordon, T., et al., 2017. Review of urban secondary organic aerosol formation from gasoline and diesel motor vehicle emissions. Environ. Sci. Technol. 51, 1074–1093.
Hoyle, C., Myhre, G., Berntsen, T., Isaksen, I., 2009. Anthropogenic influence on SOA and the resulting radiative forcing. Atmos. Chem. Phys. 9, 2715–2728.
Ji, Y., Zhao, J., Terazono, H., et al., 2017. Reassessing the atmospheric oxidation mechanism of toluene. Proc. Natl. Acad. Sci. U. S. A. 114, 8169–8174.
Li, K., Li, J., Tong, S., Wang, W., Huang, R., Ge, M., 2019. Characteristics of wintertime VOCs in suburban and urban Beijing: concentrations, emission ratios, and festival effects. Atmos. Chem. Phys. 19, 8021–8036.
Ling, Z., Xie, Q., Shao, M., et al., 2020. Formation and sink of glyoxal and methylglyoxal in a polluted subtropical environment: observation-based photochemical analysis and impact evaluation. Atmos. Chem. Phys. 20, 11451–11467.
Lu, S., Li, X., Liu, Y., Song, M., 2021. Advances on atmospheric oxidation mechanism of typical aromatic hydrocarbons. Acta Chim. Sin. 79, 1214–1431.
Lv, S., Wang, F., Wu, C., et al., 2022. Gas-to-aerosol phase partitioning of atmospheric water-soluble organic compounds at a rural site in China: an enhancing effect of NH3 on SOA formation. Environ. Sci. Technol. 56, 3915–3924.
Michoud, V., Sauvage, S., Léonardis, T., et al., 2018. Field measurements of methylglyoxal using proton transfer reaction time-of-flight mass spectrometry and comparison to the DNPH–HPLC–UV method. Atmos. Meas. Tech. 11, 5729–5740.
Mohr, C., Lopez-Hilfiker, F., Zotter, P., et al., 2013. Contribution of nitrated phenols to wood burning brown carbon light absorption in detling, United Kingdom during winter time. Environ. Sci. Technol. 47, 6316–6324.
Ng, N., Kroll, J., Chan, A., Chhabra, P., Flagan, R., Seinfeld, J., 2007. Secondary organic aerosol formation from m-xylene, toluene, and benzene. Atmos. Chem. Phys. 7, 3909–3922.
Nie, W., Yan, C., Huang, D., et al., 2022. Secondary organic aerosol formed by condensing anthropogenic vapours over China's megacities. Nat. Geosci. 15, 255–261.
Noriko, N., Janet, A., Roger, A., 2010. Formation yields of glyoxal and methylglyoxal from the gas-phase OH radical-initiated reactions of toluene, xylenes, and trimethylbenzenes as a function of NO2 concentration. J. Phys. Chem. A 114, 10140–10147.
Qi, X., Zhu, S., Zhu, C., et al., 2020. Smog chamber study of the effects of NOx and NH3 on the formation of secondary organic aerosols and optical properties from photo-oxidation of toluene. Sci. Total Environ. 727, 138632.
Rodigast, M., Mutzel, A., Herrmann, H., 2017. A quantification method for heat-decomposable methylglyoxal oligomers and its application on 1,3,5-trimethylbenzene SOA. Atmos. Chem. Phys. 17, 3929–3943.
Salvador, C., Tang, R., Priestley, M., et al., 2021. Ambient nitro-aromatic compounds – biomass burning versus secondary formation in rural China. Atmos. Chem. Phys. 21, 1389–1406.
Sander, S., Friedl, R., Ravishankara, A., Golden, D., Finlayson-Pitts, B., 2011. Chemical Kinetics and Photochemical Data for Use in Atmospheric Studies: Evaluation. number 14.
Sarwar, G., Appel, K., Carlton, A., et al., 2011. Impact of a new condensed toluene mechanism on air quality model predictions in the US. Geosci. Model Dev. 4, 183–193.
Schwantes, R., Schilling, K., McVay, R., et al., 2017. Formation of highly oxygenated low-volatility products from cresol oxidation. Atmos. Chem. Phys. 17, 3453–3474.
Seinfeld, J., Pandis, S., 2006. Atmospheric Chemistry and Physics from Air Pollution to Climate Wiley change.
Song, K., Guo, S., Wang, H., et al., 2021a. Measurement report: online measurement of gas-phase nitrated phenols utilizing a CI-LToF-MS: primary sources and secondary formation. Atmos. Chem. Phys. 21, 7917–7932.
Song, K., Guo, S., Wang, H.C., et al., 2021b. Measurement report: online measurement of gas-phase nitrated phenols utilizing a CI-LToF-MS: primary sources and secondary formation. Atmos. Chem. Phys. 21, 7917–7932.
Suh, I., Zhang, R., Molina, L., Molina, M., 2003. Oxidation mechanism of aromatic peroxy and bicyclic radicals from OH-toluene reactions. J. Am. Chem. Soc. 125, 12655–12665.
Tsiligiannis, E., Hammes, J., Salvador, C., Mentel, T., Hallquist, M., 2019. Effect of NOx on 1,3,5-trimethylbenzene (TMB) oxidation product distribution and particle formation. Atmos. Chem. Phys. 19, 15073–15086.
Volkamer, R., Jimenez, J., Martini, F., et al., 2006. Secondary organic aerosol formation from anthropogenic air pollution: rapid and higher than expected. Geophys. Res. Lett. 33 A11F 05.
Wang, G., Zhang, R., Gomez, M., et al., 2016. Persistent sulfate formation from London fog to chinese haze. Proc. Natl. Acad. Sci. U. S. A. 113, 13630–13635.
Wang, H., Gao, Y., Wang, S., et al., 2020. Atmospheric processing of nitrophenols and nitrocresols from biomass burning emissions. J. Geophys. Res. 125 e2020JD033401.
Wayne, R., Barnes, I., Biggs, P., et al., 1991. The nitrate radical: physics, chemistry, and the atmosphere. Atmos. Environ. Part A 25, 1–203.
Wu, R., Pan, S., Li, Y., Wang, L., 2014. Atmospheric oxidation mechanism of toluene. J. Phys. Chem. A 118, 4533–4547.
Wyche, K., Monks, P., Ellis, A., et al., 2009. Gas phase precursors to anthropogenic secondary organic aerosol: detailed observations of 1,3,5-trimethylbenzene photooxidation. Atmos. Chem. Phys. 9, 635–665.
Xu, L., Moller, K., Crounse, J., Kjaergaard, H., Wennberg, P., 2020. New insights into the radical chemistry and product distribution in the OH-initiated oxidation of benzene. Environ. Sci. Technol. 54, 13467–13477.
Yuan, B., Liggio, J., Wentzell, J., et al., 2016. Secondary formation of nitrated phenols: insights from observations during the Uintah Basin winter ozone study (UBWOS) 2014. Atmos. Chem. Phys. 16, 2139–2153.
Yuan, B., Koss, A., Warneke, C., Coggon, M., Sekimoto, K., de Gouw, J., 2017. Proton-transfer-reaction mass spectrometry: applications in atmospheric sciences. Chem. Rev. 117, 13187–13229.
Zaytsev, A., Koss, A., Breitenlechner, M., et al., 2019. Mechanistic study of the formation of ring-retaining and ring-opening products from the oxidation of aromatic compounds under urban atmospheric conditions. Atmos. Chem. Phys. 19, 15117–15129.
Zhang, X., Cappa, C., Jathar, S., et al., 2014. Influence of vapor wall loss in laboratory chambers on yields of secondary organic aerosol. Proc. Natl. Acad. Sci. U. S. A. 111, 5802–5807.
Zhang, R., Wang, G., Guo, S., et al., 2015. Formation of urban fine particulate matter. Chem. Rev. 115, 3803–3855.
Zhang, Q., Sarkar, S., Wang, X., et al., 2019. Evaluation of factors influencing secondary organic carbon (SOC) estimation by CO and EC tracer methods. Sci. Total Environ. 686, 915–930.
Zhang, J., Choi, M.S., Ji, Y.M., Zhang, R.Y., Zhang, R.Q., Ying, Q., 2021. Assessing the uncertainties in ozone and SOA predictions due to different branching ratios of the cresol pathway in the toluene-OH oxidation mechanism. ACS Earth. Space. Chem. 5, 1958–1970.